# Detection of Thermal Effluent Discharge Using Sea Surface Nautical Radar Images

Hsiang-Yu Bau, Li-Chung Wu, and Laurence Zsu-Hsin Chuang

***Abstract*—This letter presents the patterns of thermal effluent discharge determined by sea surface images that are acquired by nautical X-band radar. By averaging the sequential image series, we detect an obvious echo band pattern at the drain outlet of a power plant. The detection of microscale (less than 1 km) thermal effluent features using the low-grazing-angle nautical radar approach has received little attention up to now. The field sea surface temperature data confirmed that the echo band matches the spatial distribution of the thermal effluent discharge. By observing hourly image cases, we also confirm that this echo band moves approximately two times per day and that this oscillation is dominated by the tidal current.**

***Index Terms*—Sea surface pattern, thermal effluent discharge, X-band radar.**

## I. Introduction

NAUTICAL X-band radar, which is normally used to detect the coastline and obstacles on the sea surface, is currently one of the most popular tools for ocean remote sensing. Different studies have confirmed the mechanism for imaging sea surface wind waves and swell patterns by means of X-band radar [1], [2]. Based on the principle of sea surface wave imaging, the feasibility of ocean wave observation was also demonstrated [3]. Following this research [3], some other studies proposed different algorithms to derive the information of sea surface wind, current, and bathymetry from the gravity wave patterns on the X-band radar images [4]–[6]. In addition to the applications of wind, wave, current, and bathymetry monitoring, the X-band radar echo images also provide other significant information related to different physical features, such as internal and breaking waves and river plume front at estuary areas [7]–[9]. In addition to the aforementioned information, we also noticed that the pattern of the thermal effluent discharge on the sea surface images can be observed. For the operation of a power plant, the release of thermal energy into the ocean is quite common. To clarify the impact of waste heat on the coastal environment, monitoring the thermal effluent is often necessary. To obtain the thermal effluent information, we cannot ignore the interaction between the thermal effluent and the environmental factors. Some moving features of the thermal effluent, such as diffusion and oscillation, are unavoidable in the sea area. To monitor the spatial features of the thermal effluent, some studies rely on large numbers of water temperature gauges [10].

Compared with *in situ* measurements, remote sensing is an ideal way to obtain the spatial information of the thermal effluent. Airborne- and satellite-based technologies have been used to monitor the surface thermal front in different studies. Nghiem *et al.* [11] reported that the sea surface temperature front can be detected with backscatter data at large incidence angles (incidence angles larger than 20° and smaller than 60°) for various wind directions over the cold and warm sides by the Ku-band scatterometer. Askari *et al.* [12] investigated the physics of radar backscatter across sea surface temperature fronts using a simple drag model followed by airborne X-band radar observations. Askari *et al.* [12] also reported that the changes in atmospheric stratification resulting from changes in sea surface temperature caused the change in the surface wind stress; hence, the change in surface roughness driven by the stress variability is one of the dominant ingredients in the imaging of mesoscale frontal boundaries. The surface thermal fronts that were discussed by these two studies [11], [12] are the Gulf Stream and the warm core ring, whose scales are much larger than the thermal effluent from a power plant. Compared with the airborne- and satellite-based technologies, the land-based remote sensing primarily works in the low-grazing-angle mode. The advantage of land-based remote sensing is the continuous and long-term monitoring. Hence, we could obtain spatiotemporal information from the image sequences. However, the detection of microscale thermal effluent features using the low-grazing-angle nautical radar approach has received little attention. The aim of our study is to discuss the sea surface patterns observed in coastal X-band radar images to determine the practicability of detecting microscale (less than 1 km) thermal effluent patterns using X-band radar.

## II. Data Source

The image cases in our study are collected from a nautical X-band radar station that is installed on the western coast of Taiwan (22.861° N and 120.194° E). The radar antenna is at an altitude of 15 m. Because the location of the thermal effluent is at least 500 m from the radar antenna, the radar grazing angle is less than 2°. For the image formats in our study, 64 continuous radar image sequences with a 7.5-m/pixel spatial resolution are acquired for each measurement. The radar device is equipped with a 42-r/min antenna, which yields an image sequence sampling rate of 0.7 Hz.

Manuscript received May 21, 2012; revised July 25, 2012; accepted August 6, 2012. This work was supported in part by the National Science Council under Grant NSC 98-2923-I-006-001-MY4 and Grant NSC 100-2221-E-006-020 and in part by the Taiwan Ocean Research Institute under Grant TORI-P-099074.

H.-Y. Bau and L. Z.-H. Chuang are with the Institute of Ocean Technology and Marine Affairs, National Cheng Kung University, Tainan 70101, Taiwan (e-mail: hypau@tori.narl.org.tw; zsuhsin@mail.ncku.edu.tw).

L.-C. Wu is with the Coastal Ocean Monitoring Center, National Cheng Kung University, Tainan 70101, Taiwan (e-mail: jackalson18@gmail.com).

Digital Object Identifier 10.1109/LGRS.2012.2215912

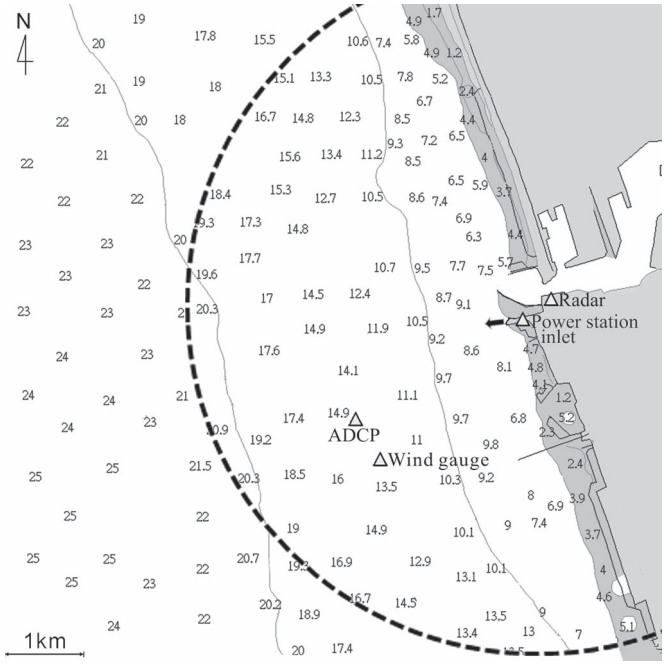


Fig. 1. Experimental site of our study (water depth unit: In meters). The arrow in the figure indicates the direction of prevailing currents at the tidal inlet.

Fig. 1 shows the sea area of our experiment, in which the radar monitoring area is marked by a dashed circle. To verify the features from the sea surface radar images, the simultaneous *in situ* water elevation and current data obtained from a bottom-mounted acoustic doppler current profiler (ADCP) were used.

## III. Image Processing for Detecting Thermal Effluent Features

The X-band radar that is used in our study is part of a noncoherent system, which means that the information we need is only acquired from the radar echo intensity, and we do not process the phase information from the radar signals. As aforementioned, every image case contains 64 continuous radar image sequences. The patterns of high-frequency fluctuation, which are due to wind waves and swells, are often visible on the single-frame image.

To eliminate the spatial patterns of gravity waves from the sea surface images, we average the sequential images from 64 continuous image series. To analyze the radar backscatter from the averaged images, we normalize the radar echo intensity first as follows:

$$I_n(x,y) = I(x,y)/I_{\max} \tag{1}$$

where $I(x,y)$ is the original averaged radar echo intensity at different spatial locations $(x,y)$, $I_n(x,y)$ is the normalized result from $I(x,y)$, and $I_{\max}$ is the maximal value of the entire $I(x,y)$. Note that the maximal values of the different image cases are always at the location of the radar antenna. Because all of the radar backscatter images are obtained from the same radar system, the values of $I_{\max}$ are also nearly the same among the different image cases.

Based on the radar equation, the radar echo intensity is related to the distance $R$ between the target and the radar antenna. The power of the signal reflected from the target and received by the radar is proportional to $R^{-4}$. Since the thermal effluent patterns on our radar image cases are all within 2.5 km from the radar antenna, the thermal effluent patterns within this range are clear enough to be recognized. Hence, our study does not deal with the decay effect with increasing distance. Fig. 2 presents a radar image case in our study. In Fig. 2(a), there is obvious radar echo intensity at the middle part of the radar image. The drain outlet of a power plant is at the right-hand side of this area. From the features of the radar echo intensity, we can identify that the obvious radar echo band on the sea surface flows toward the north. Fig. 2(b) presents the result of near simultaneous *in situ* sea surface temperature data, which is nested on the sea surface image. The temperature data were measured by a small boat, and all the data were collected within 1 h. These data present the sea surface temperature over a short duration. From the *in situ* temperature data information in Fig. 2(b), we notice an obvious warm band from the zone of the drain outlet that is directed to the north. The averaged sea surface temperature within the entire data set is approximately 29 °C. However, the temperature value within this warm water area can be up to 31 °C. We also notice the area of the obvious radar echo band on the sea surface image is located within this warm water zone.

To focus on the radar echo features within the effluent area, we select a subimage area from the area near the drain outlet. Fig. 3 presents the image cases within a continuous 24 h. The results show that the radar echo band oscillates with time. In addition to the radar echo band, speckles are present on the sea surface images. To enhance the pattern of the thermal effluent, we adjusted the image intensity values. Because we normalized the intensities of every image case by (1), the normalized intensities are within the range of [0 1]. To enhance the intensities of the thermal effluent band, we mapped the intensity values within the range of [0.7 1] to new values within the range of [0 1]. After this process, some of the intensity values are saturated over a larger range of intensity values.

Fig. 4 presents the results of the image intensity adjustment from Fig. 3. As shown in Fig. 2, the radar antenna is installed at the north of the drain outlet. The distances between the radar antenna and the thermal effluent echo bands, which bend to the south, are longer. Because the received electromagnetic energy obeys a decay law with increasing distance, the intensity values of the echo band are stronger at the north of the drain outlet.

From the images in Fig. 4, we can more easily identify the radar echo band. For the subimage cases at 00, 01, 11, 12, 13, 14, and 15 o'clock, the radar echo bands of these cases bend toward the north. We classified these images as cases (A). However, the radar echo bands from the subimage cases at 07, 08, 18, 19, 20, 21, and 22 o'clock bend from the location of the drain outlet toward the south. We classified these images as cases (B). To interpret the moving features of the echo band, we utilize the simultaneous *in situ* tide and current measurements from the ADCP. Fig. 5 shows the time series of the sea elevation, current speed, and current direction. The time

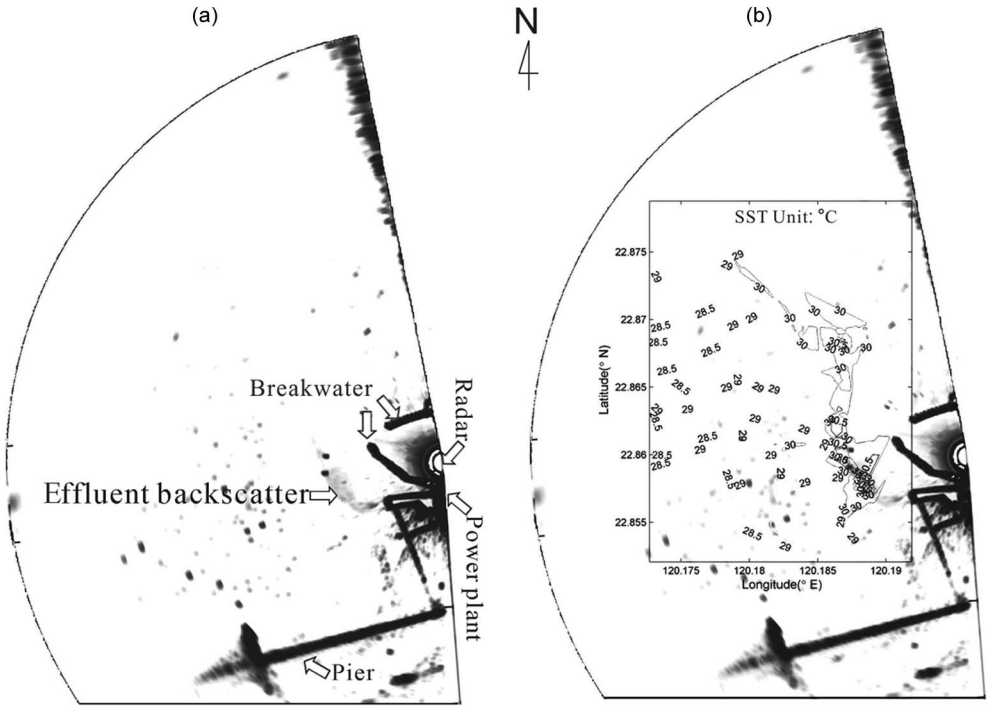


Fig. 2. Image case of the thermal effluent pattern. An obvious warm band was noticed from the zone of the drain outlet that is directed to the north: The area of the obvious radar echo band on the sea surface image is located within this warm water zone.

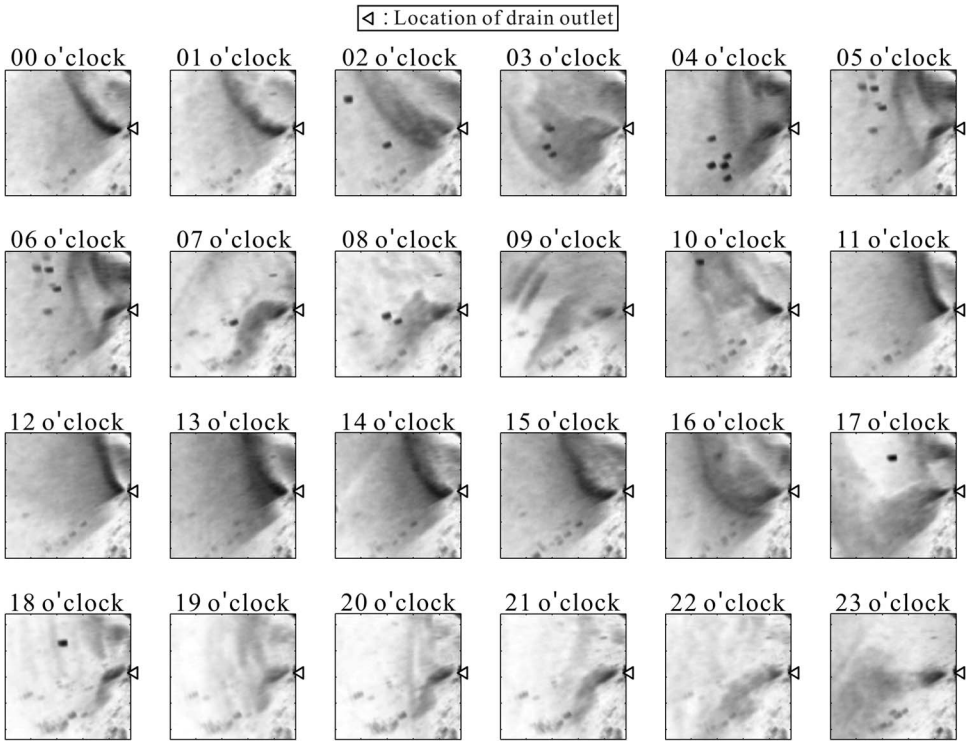


Fig. 3. Image cases of the thermal effluent features within a continuous 24 h. The size of every subimage is approximately 1 km × 1 km. The location of the drain outlet is at the middle position of the right margin of every subimage. The results show that the radar echo band oscillates with time. However, the effluent features are not clear due to the influences of noise.

ranges of cases (A) and cases (B) are also indicated in Fig. 5. We notice that cases (A) often occur while the tide changes from low water to high water and that the current directions are often approximately north-northeast. Compared with cases (A), cases (B) often occur as the tide changes from high water to low water, and the current direction moves to east-southeast. We can confirm that the thermal effluent echo band oscillations are due to the influence of the tide and current.

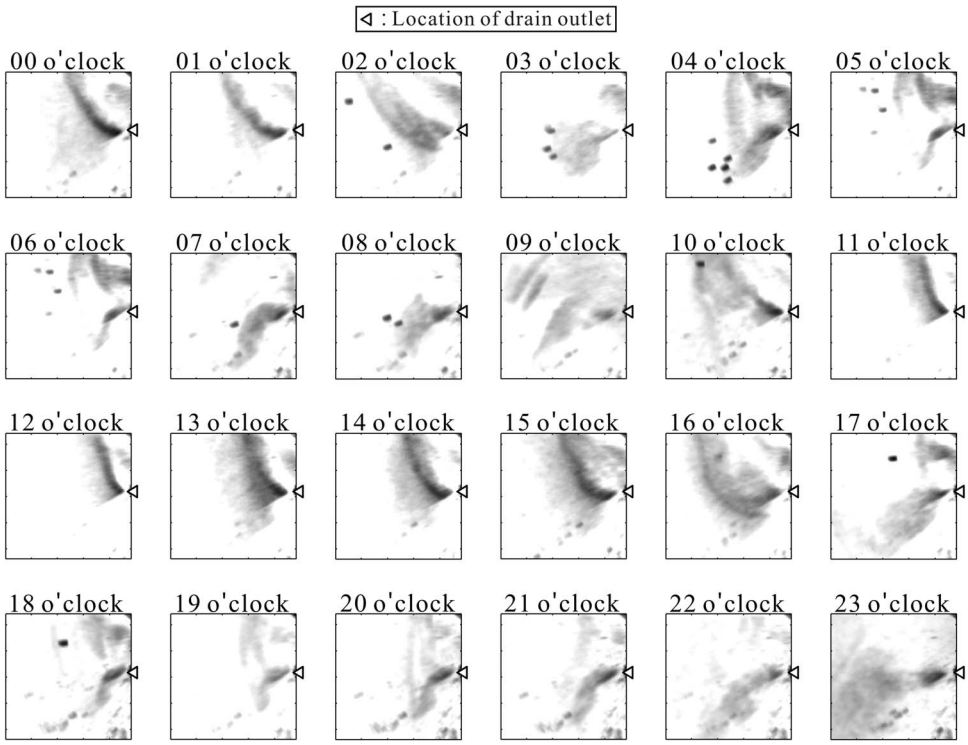


Fig. 4. Image cases of the thermal effluent features after adjusting the image intensity values. The intensity values of the radar echo band, which bend to the north, are stronger than the radar echo band, which bends to the south.

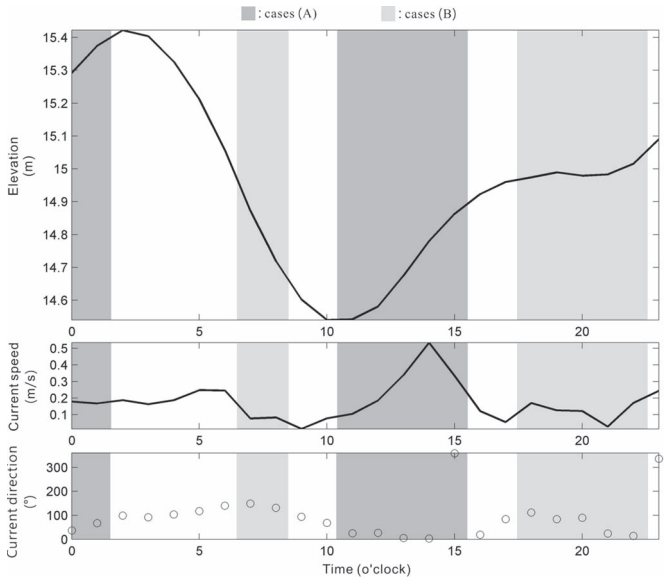


Fig. 5. Tide and near sea surface current data measured from the ADCP. For the definition of current direction, 0° means that the current flows from the south to the north, and 90° means that the current flows from the west to the east.

## IV. Conclusion

Monitoring the thermal effluent discharge that is produced from the power plant is a key to understanding the impact of waste heat on the coastal environment. *In situ* measurement of water temperature is a common technique for obtaining field information on the thermal effluent. However, it is difficult to obtain spatial information using only a few *in situ* sensors. Remote sensing is a potential technology for obtaining high-resolution spatial ocean surface information.

In our study, we noticed that the thermal effluent pattern can be detected from nautical X-band radar images. Other studies have reported that the change of sea surface temperature would influence sea surface roughness and that radar backscattering is influenced by the sea surface roughness. However, the detection of microscale thermal effluent features on the sea surface, such as those from the thermal effluent of a power plant, by using nautical radar images has received little attention. Here, we studied the sea surface patterns obtained using coastal X-band radar images to confirm the practical use of X-band radar images for detecting microscale thermal effluent features. After comparing the *in situ* temperature data with the X-band radar images, we confirmed the feasibility of detecting the thermal effluent discharge by the X-band radar images. By observing hourly continuous image cases, we determined that the oscillation of the thermal effluent pattern is dominated by the tidal current.

In summary, we have confirmed the feasibility of detecting the thermal effluent pattern by using X-band radar images. Although our study does not determine the water temperature values from the radar image pattern, we can obtain the location and the features of motion of the thermal effluent band. This spatial information is useful for coastal management and environmental protection.

## References

[1] P. H. Y. Lee, J. D. Barter, K. L. Beach, B. M. Lake, H. Rungaldier, H. R. Thompson, and R. Yee, "Scattering from breaking gravity waves without wind," *IEEE Trans. Antennas Propag.*, vol. 46, no. 1, pp. 14–26, Jan. 1998.

[2] M. B. Kanevsky, *Radar Imaging of the Ocean Waves*. Oxford, U.K.: Elsevier, pp. 9–24.

[3] I. R. Young, W. Rosenthal, and F. Ziemer, "A three-dimensional analysis of marine radar images for the determination of ocean wave directionality and surface currents," *J. Geophys. Res.*, vol. 90, no. C1, pp. 1049–1059, Jan. 1985.
[4] H. Dankert and J. Horstmann, "A marine radar wind sensor," *J. Atmos. Ocean. Technol.*, vol. 24, no. 9, pp. 1629–1642, Sep. 2007.
[5] C. M. Senet, J. Seemann, S. Flampouris, and F. Ziemer, "Determination of bathymetric and current maps by the method DiSC based on the analysis of nautical X-band radar image sequences of the sea surface (November 2007)," *IEEE Trans. Geosci. Remote Sens.*, vol. 46, no. 8, pp. 2267–2279, Aug. 2008.
[6] S. Flampouris, J. Seemann, C. Senet, and F. Ziemer, "The influence of the inverted sea wave theories on the derivation of coastal bathymetry," *IEEE Geosci. Remote Sens. Lett.*, vol. 8, no. 3, pp. 436–440, May 2011.
[7] I. S. Robinson, N. P. Ward, C. P. Gommenginger, and M. A. Tenorio-Gonzales, "Coastal oceanography applications of digital image data from marine radar," *J. Atmos. Ocean. Technol.*, vol. 17, no. 5, pp. 721–735, May 2000.
[8] R. J. Ramos, B. Lund, and H. C. Graber, "Determination of internal wave properties from X-band radar observations," *Ocean Eng.*, vol. 36, no. 14, pp. 1039–1047, Oct. 2009.
[9] P. A. Hwang, M. A. Sletten, and J. V. Toporkov, "Breaking wave contribution to low grazing angle radar backscatter from the ocean surface," *J. Geophys. Res.*, vol. 113, no. C9, pp. C0 901-1–C0 901-12, 2008.
[10] M. Kailasam and S. Sivakami, "Effect of thermal effluent discharge on benthic fauna off Tuticorin bay, south east coast of India," *Indian J. Marine Sci.*, vol. 33, no. 2, pp. 194–201, Jun. 2004.
[11] S. V. Nghiem, F. K. Li, E. J. Walsh, and S.-h. Lou, "Radar backscatter across the Gulf Stream sea surface temperature front," *IEEE Trans. Geosci. Remote Sens.*, vol. 38, no. 2, pp. 926–941, Mar. 2000.
[12] F. Askari, G. L. Geernaeft, W. C. Keller, and S. Raman, "Radar imaging of thermal fronts," *Int. J. Remote Sens.*, vol. 14, no. 2, pp. 275–294, 1993.